Neutron diffraction studies of the crystalline and magnetic properties of UFe_2

1989 J. Phys.: Condens. Matter 1 10229

(http://iopscience.iop.org/0953-8984/1/51/002)

J. Phys.: Condens. Matter **1** (1989) 10229–10248. Printed in the UK

Neutron diffraction studies of the crystalline and magnetic properties of UFe_2

B Lebech†, M Wulff‡‖, G H Lander‡, J Rebizant‡, J C Spirlet‡ and A Delapalme§

† Physics Department, Risø National Laboratory, DK-4000 Roskilde, Denmark

‡ Commission of the European Communities, JRC, Institute for Transuranium Elements, Postfach 2340, D-7500 Karlsruhe, Federal Republic of Germany

§ Laboratoire Léon Brillouin, Centre d'Études Nucléaires Saclay, 91191 Gif-sur-Yvette, France

Received 10 April 1989

Abstract. Studies using both polarised and unpolarised neutrons have been performed on single crystals of the Laves phase intermetallic compound UFe_2. We describe studies of the twinning characteristics (two crystals with a common ⟨1,1,1⟩ axis) of our sample, a feature that is probably common in these cubic compounds. We then describe studies with polarised neutrons to determine the magnitude of the spin and orbital moments on the uranium site. In agreement with a recent theoretical prediction these two moments are found to be almost equal, but oppositely directed in real space. The net moment at the U site is only 0.01 μ_B. The polarised neutron experiments also allow us to put an upper limit on any possible anisotropy in the magnetisation. High-field magnetisation experiments up to (20 T) on the same crystal as used in the neutron experiments allow us to determine the conduction–electron polarisation.

1. Introduction

Recent advances in band-structure calculations (Eriksson *et al* 1986, Boring *et al* 1987) have permitted a realistic treatment of intermetallic compounds containing 5f actinide elements (U, Np, Pu, etc) and the magnetic 3d transition elements (Mn, Fe, Co and Ni). These calculations suggest that the 5f electrons are itinerant in nature and often hybridise strongly with the itinerant 3d electrons. Furthermore, the calculations can predict the lattice parameters, whether the compounds exhibit spontaneous magnetic order or not, and compound properties such as the bulk moduli. To examine the microscopic magnetic properties Brooks *et al* (1988) have succeeded in adding spin–orbit coupling into the band-structure calculations. This results in good agreement between theory and experiment (Franse 1983) for properties such as total moment, electronic specific-heat coefficient and the pressure dependence of the magnetic moment in, for instance, UFe_2. In addition, Brooks *et al* (1988) have recently made an important prediction concerning the magnetic moment at the uranium site. They find that the hybridisation reduces disproportionately the orbital moment, which usually dominates the total moment in

‖ Present address: Laboratoire de Diffraction Neutronique, Département de Recherche Fondamentale, CENG, 85-X-38041, Grenoble Cédex, France.

0953-8984/89/5110229 + 20 $02.50

uranium compounds, and because of this the orbital moment is predicted to become comparable to the spin moment in UFe_2. Furthermore, the net spin and orbital moments are directed *antiparallel* in U compounds so that the prediction for UFe_2 is that the small moment known to be present on the U site (Yessik 1969, Lander *et al* 1977) comes from the almost complete cancellation of two larger, but oppositely directed, components.

These predictions, particularly those concerning the cancellation of the spin and orbital moments, led us to re-examine UFe_2 and to search for this effect with neutron scattering. We have, indeed, found such a dramatic cancellation with $\mu_l = 0.23(1)\ \mu_B$ and $\mu_s = -0.22(2)\ \mu_B$ for the orbital and spin components, respectively. The magnetic form factor corresponding to this 'cancellation' effect has a most unusual shape, and brief reports of this have been published (Wulff *et al* 1989a, b). In this paper we discuss the experiments in more detail, and in particular how we dealt with the existence of 'twinning' in our crystals. Although normally a disadvantage, by understanding this mechanism we were able to use it to make detailed investigations of the magnetic anisotropy in UFe_2.

2. Unpolarised neutron study

UFe_2 crystallises in the cubic FCC Laves phase and is ferromagnetic below 160 K. The neutron study was performed on a single crystal cut from a larger boule grown by the Czochralski technique. Prior to the polarised neutron study, the crystal was completely characterised using the four-circle diffractometer situated at the DR3 reactor at Risø National Laboratory, Denmark. The crystal was found to be perfectly twinned along a $\langle 1,1,1 \rangle$ axis with two nearly equally sized twins (A and B) turned 60° relative to each other (see figure 1). This type of twinning is not uncommon in FCC crystals (see, e.g., Steigenberger *et al* 1986, Giebultowicz *et al* 1989), although one usually selects untwinned crystals for diffraction studies because the data analysis is more straightforward. However, for the polarised neutron study of Wulff *et al* (1989a) it was not possible to get a sufficiently large untwinned crystal of UFe_2, and therefore a complete understanding of the geometry of the twinned crystal was necessary. Below we give details of the four-circle study and the subsequent analysis. The analysis shows that it is possible, with reasonable accuracy, to perform a full least-squares refinement of a set of structural data

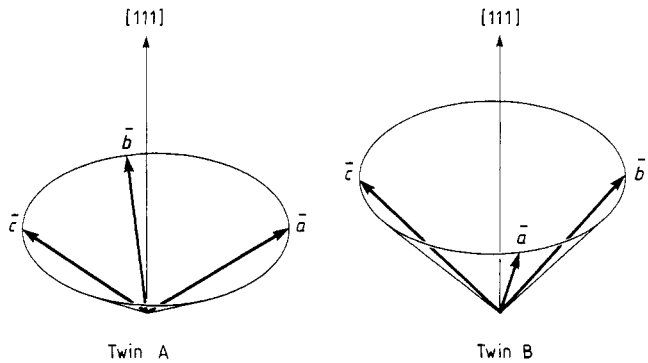

Figure 1. Illustration of the relative orientation of the main cubic axes of twin A and B. The twin axis is the [1,1,1] body diagonal.

collected on a twinned crystal. In § 2.1 we outline some fundamental geometrical properties of twinned face-centred cubic crystals, which may be useful in similar studies. From a crystallographer's point of view, the analysis may seem straightforward because of the relatively simple crystal structure of UFe_2. However, for a study of the magnetic structure, the description of the analysis is important. The reason for this is that in magnetic studies it is common to apply a magnetic field along a particular crystallographic axis. If the crystal is twinned, the result may then be that the field is applied along different crystallographic axes in the different twin components and this causes the magnetic response to differ for the different twin components. Therefore, data analysis without a complete understanding of the twinned crystal may be misleading, particularly if the system is magnetically anisotropic.

2.1. Transformation from a cubic to a hexagonal unit cell

As mentioned above, twinning in face-centred cubic crystals is rather common and often found in the large crystals used for neutron diffraction experiments; the twin axis is usually a $\langle 1, 1, 1\rangle$ axis. Either perfect or imperfect twinning occurs. In the latter case the twin axes are slightly misaligned, and the twinning may be observed easily because some of the Bragg peaks will be split in some directions of reciprocal space. In the former case, the twin axes are perfectly aligned, and twinning may be difficult to detect in a large mosaic crystal, especially if the detailed crystal structure is unknown.

For UFe_2 the twinning was found to be perfect in the sense defined above. In order to check experimentally for this kind of twinning, it is useful to describe the FCC cell in terms of the corresponding hexagonal close-packed pseudo-cell and search for reflections which are allowed by the hexagonal symmetry but forbidden by the cubic symmetry. If such reflections are observed, they will be evidence of perfect twinning provided the crystal structure of the untwinned crystal is face-centred cubic. Below we derive the tools necessary to transform the unit cell of the original cubic crystal (twin A) to the corresponding cubic cell for twin B via a hexagonal pseudo-cell which combines both twins.

Figure 2 defines the FCC unit cell with $a_c = b_c = c_c$. It also shows the axes of the hexagonal pseudo-cell for twin A, $a_h^A = b_h^A$ and c_h^A with the [1, 1, 1] axis as the twin axis.

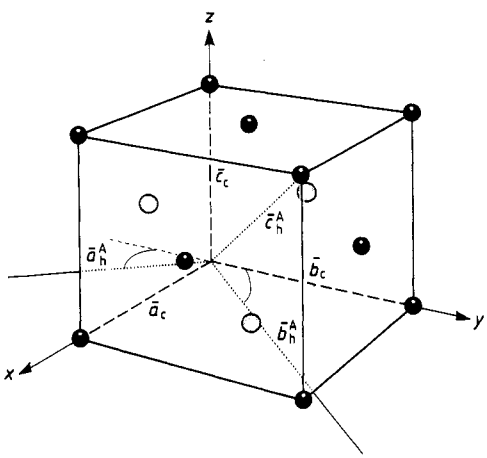

Figure 2. Definition of the FCC unit cell ($a_c = b_c = c_c$) and the axes of the hexagonal pseudo-cell for twin A ($a_h^A = b_h^A = \sqrt{2}/2\, a_c$ and $c_h^A = \sqrt{3} a_c$) for a [1,1,1] twin axis. For twin A the hexagonal axes are given by $a_h^A = \frac{1}{2}a_c - \frac{1}{2}b_c$, $b_h^A = \frac{1}{2}b_c - \frac{1}{2}c_c$ and $c_h^A = a_c + b_c + c_c$.

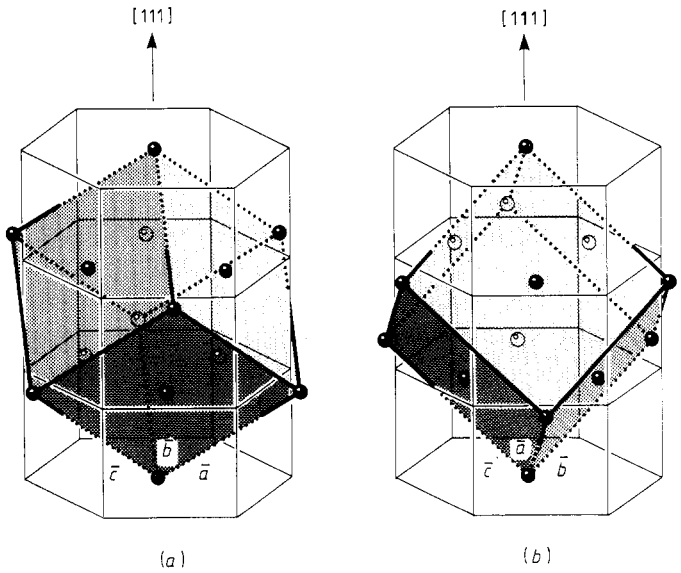

Figure 3. Illustration of the orientations of (*a*) twin A and (*b*) twin B in the hexagonal pseudo-cell. The full circles are visible atoms of an FCC structure, the dotted circles are hidden atoms of an FCC structure.

For twin A, the hexagonal axes are given by

$$a_h^A = \tfrac{1}{2}a_c - \tfrac{1}{2}b_c \qquad b_h^A = \tfrac{1}{2}b_c - \tfrac{1}{2}c_c \qquad c_h^A = a_c + b_c + c_c. \tag{1}$$

However, we could equally well have chosen

$$a_h^B = \tfrac{1}{2}a_c - \tfrac{1}{2}c_c \qquad b_h^B = -\tfrac{1}{2}a_c + \tfrac{1}{2}b_c \qquad c_h^B = a_c + b_c + c_c \tag{2}$$

which corresponds to a 60° rotation around [1,1,1] of the basal plane axes (a_h^A, b_h^A). The set of axes (a_h^B, b_h^B, c_h^B) defines twin B. Figure 3 shows the orientations of twins A (figure 3(*a*)) and B (figure 3(*b*)) in the same real-space hexagonal pseudo-cell. A perfect [1,1,1] twin may be visualised as a random stacking of twin-A and twin-B unit cells.

From equations (1) and (2) it is easy to deduce the matrices transforming the cubic Miller indices of twins A or B to the Miller indices of the hexagonal pseudo-cell ($\{A\}_A$ and $\{A\}_B$) and vice versa ($\{B\}_A$ and $\{B\}_B$). The resulting matrices are quoted in the top part of table 1. Also quoted in table 1 are the equivalent matrices for other choices of the common ⟨1,1,1⟩-type twin axis. Another useful set of transformation matrices is quoted in table 2. The matrices $\{C\}$ and $\{D\}$ may be used to transform the cubic Miller indices of the cubic twin-B unit cell to Miller cubic indices of the cubic twin-A unit cell and vice versa. For a common [1,1,1] twin we find, as expected, that the (1,1,1) reflection of twin B will overlap with the (1,1,1) reflection of twin A.

Using the matrices quoted in tables 1 and 2, it is easy to calculate the Miller indices of, for instance, twin A either in terms of the unit cell for twin B or in terms of the hexagonal pseudo-cell. By means of table 1, it is easily verified, for example, that for a [1,1,1] twin axis the (1,1,1) cubic reflection for both twin A and twin B transforms to the (0,0,3) hexagonal reflection, whereas the $(\bar{1},1,1)$, $(1,\bar{1},1)$ and $(1,1,\bar{1})$ cubic reflections of twin A transform to the $(\bar{1},0,1)$, $(1,\bar{1},1)$ and (0,1,1) hexagonal reflections and the $(\bar{1},1,1)$,

Table 1. Transformation from cubic to hexagonal Miller indices and vice versa.

Common cubic axis	Twin A						Twin B					
	$\{A\}_A$ Cubic → hexagonal			$\{B\}_A$ Hexagonal → cubic			$\{A\}_B$ Cubic → hexagonal			$\{B\}_B$ Hexagonal → cubic		
111	1/2	0	1	4/3	−2/3	−2/3	1/2	−1/2	1	2/3	2/3	−4/3
	−1/2	1/2	1	2/3	2/3	−4/3	0	1/2	1	−2/3	4/3	−2/3
	0	−1/2	1	1/3	1/3	1/3	−1/2	0	1	1/3	1/3	1/3
$\bar{1}11$	−1/2	0	−1	−4/3	−2/3	−2/3	0	−1/2	−1	−2/3	2/3	−4/3
	0	−1/2	1	−2/3	−4/3	2/3	1/2	−1/2	1	−4/3	−2/3	−2/3
	−1/2	1/2	1	−1/3	1/3	1/3	−1/2	0	1	−1/3	1/3	1/3
$1\bar{1}1$	1/2	−1/2	1	2/3	4/3	2/3	1/2	0	1	4/3	2/3	−2/3
	1/2	0	−1	−2/3	2/3	4/3	0	1/2	−1	2/3	4/3	2/3
	0	1/2	1	1/3	−1/3	1/3	−1/2	1/2	1	1/3	−1/3	1/3
$11\bar{1}$	−1/2	0	1	−4/3	2/3	−2/3	0	−1/2	1	−2/3	−2/3	−4/3
	0	1/2	1	−2/3	4/3	2/3	−1/2	1/2	1	−4/3	2/3	−2/3
	−1/2	1/2	−1	1/3	1/3	−1/3	−1/2	0	−1	1/3	1/3	−1/3

$$\begin{Bmatrix} h_h \\ k_h \\ l_h \end{Bmatrix} = \{A\}\{h_c, k_c, l_c\}; \begin{Bmatrix} h_c \\ k_c \\ l_c \end{Bmatrix} = \{B\}\{h_h, k_h, l_h\}; \{A\} = \{B\}^{-1}.$$

Table 2. Transformation of cubic twin-A Miller indices to cubic twin-B Miller indices and vice versa.

Common cubic axis	Twin B → twin A, $\{C\}$			Twin A → twin B, $\{D\}$		
111	2/3	−1/3	2/3	2/3	2/3	−1/3
	2/3	2/3	−1/3	−1/3	2/3	2/3
	−1/3	2/3	2/3	2/3	−1/3	2/3
$\bar{1}11$	2/3	1/3	−2/3	2/3	−2/3	1/3
	−2/3	2/3	−1/3	1/3	2/3	2/3
	1/3	2/3	2/3	−2/3	−1/3	2/3
$1\bar{1}1$	2/3	1/3	2/3	2/3	−2/3	−1/3
	−2/3	2/3	1/3	1/3	2/3	−2/3
	−1/3	−2/3	2/3	2/3	1/3	2/3
$11\bar{1}$	2/3	−1/3	−2/3	2/3	2/3	1/3
	2/3	2/3	1/3	−1/3	2/3	−2/3
	1/3	−2/3	2/3	−2/3	1/3	2/3

$$\begin{Bmatrix} h_A \\ k_A \\ l_A \end{Bmatrix} = \{C\}\{h_B, k_B, l_B\}; \begin{Bmatrix} h_B \\ k_B \\ l_B \end{Bmatrix} = \{D\}\{h_A, k_A, l_A\}; \{C\} = \{D\}^{-1}.$$

$(1,\bar{1},1)$ and $(1,1,\bar{1})$ cubic reflections of twin B transform to the $(\bar{1},1,1)$, $(0,\bar{1},1)$ and $(1,0,1)$ hexagonal reflections. This means that both twins contribute to the Bragg scattered intensity observed in the (1,1,1) cubic reflection while only one twin contributes to the intensity of the $\langle\bar{1},1,1\rangle$-type cubic reflections. However, if the twins have equal size, there will be apparent six-fold symmetry around the [1,1,1] twin axis ([0,0,3] hexagonal axis).

Table 3. Examples of Miller indices for twin-A reflections transformed to Miller indices of twin-B unit cell and the hexagonal pseudo-cell for a $[11\bar{1}]$ twin axis.

Cubic twin-A cell			Cubic twin-B cell			Hexagonal cell		
1	1	1	−1/3	5/3	1/3	−1	1	1
−1	1	1	−5/3	1/3	−1/3	0	1	−1
1	−1	1	1/3	1/3	5/3	−1	0	−1
1	1	−1	1	1	−1	0	0	3
3	3	3	−1	5	1	−3	3	3
−3	3	3	−5	1	−1	0	3	−3
3	−3	3	1	1	5	−3	0	−3
3	3	−3	3	3	3	0	0	9
2	2	0	2/3	8/3	−2/3	−1	0	4
0	2	2	−2	2	0	−1	2	0
2	0	2	0	2	2	−2	1	0
2	−2	0	2	0	2	−1	−1	0
0	2	−2	2/3	2/3	−8/3	1	0	4
2	0	−2	8/3	2/3	−2/3	0	−1	4
4	0	0	8/3	8/3	5/3	−2	0	4
0	4	0	−5/3	8/3	8/3	0	2	4
0	0	4	−8/3	5/3	8/3	−2	2	−4

The use of table 2 is illustrated in table 3 for a $[1,1,\bar{1}]$ twin axis, which is the twin axis in the present experiment. Inspection of this table shows that the reflections of twin A will be described by either integer or non-integer Miller indices of the cubic twin-B cell. Reflections from twin A of the latter type will of course *not* coincide with reflections from twin B. However, reflections from twin A of the former type will coincide with reflections from twin B, but not necessarily with the same type of reflections. Note for instance that in the cubic notation, the (3,3,3) twin-A reflection will coincide with the $(\bar{1},5,1)$ twin-B reflection while the $(3,3,\bar{3})$ reflections from both twin A and twin B coincide.

We have now derived the necessary transformations (tables 1 and 2) and in the following we will consider the four-circle measurements on UFe_2 and the subsequent analysis.

2.2. *Experimental details for the x-ray and the unpolarised neutron studies*

A small crystal cut from the large UFe_2 boule was used in an x-ray study. The results of this study agreed well with the cubic FCC Laves phase structure Fd3m ($a_0 = 7.055(2)$ Å) with the U atoms in the (8*a*) positions (1/8,1/8,1/8; 7/8,7/8,7/8; + FCC) and the Fe atoms in the (16*d*) positions (1/2,1/2,1/2; 1/2,1/4,/1/4; 1/4,1/2,1/4; 1/4,1/4,1/2; +FCC). The *R* factor for the x-ray study was 2.1%, allowing little doubt that, for the crystal used in the x-ray study, the cubic Laves phase is the correct structure at room temperature. In addition, a powder x-ray study showed no extra lines which indicated that the material was single phase.

The single crystal used for the neutron study was cut from the same boule of UFe_2 as that used for the x-ray study. It was cut as a cylinder of ~4 mm diameter and ~3 mm height and mounted with the cylinder axis parallel to the ω axis of the four-circle instrument. The cylinder axis is close to, but not exactly parallel to, a $\langle 111 \rangle$-type crystal axis. Two different unpolarised neutron studies were made, a room-temperature crystallographic study and measurement of the temperature dependence of the intensity in selected Bragg peaks. For the latter experiment the crystal was mounted at the four-circle in a Displex cryostat (Henriksen *et al* 1986). This allowed data collection from room temperature down to 10 K and made it possible to study the temperature variation of the magnetic moment in UFe_2 (see § 4 and figure 8).

The purpose of the room-temperature study to be described in the remaining part of § 2) was to characterise the crystal and determine the stoichiometry. The crystal was easily oriented with well shaped gaussian Bragg peaks (figure 4). However, on comparing the intensity of equivalent reflections $\langle h, k, l \rangle$, the intensities generally fell into two groups, one group with strong peaks and one with weak peaks. The ratio between the intensity of the two groups of equivalent reflections was close to two, and Friedel pairs had equal intensity within statistics. A few examples of measured intensities are quoted in table 4. When comparing the intensities of the four $\langle 1,1,1 \rangle$ (or four $\langle 2,2,2 \rangle$) reflections, it seemed relevant to conclude that the crystal has a preferred [1,1,1] cubic axis with apparent three-fold symmetry. A systematic search at $(\omega, 2\theta)$ for (2,2,0)-type reflections with χ fixed ($-92° < \chi > 43°$ in steps of 6°) and φ varying from 180° to −179° for each setting of χ resulted in finding seven pairs of reflections related by Friedel's law and two reflections for which the Friedel-related reflections were outside the χ-range covered by the systematic scans; i.e. the systematic search revealed nine pairs of reflections (three strong, six weak) which could be indexed as (2,2,0)-type reflections, not six pairs as

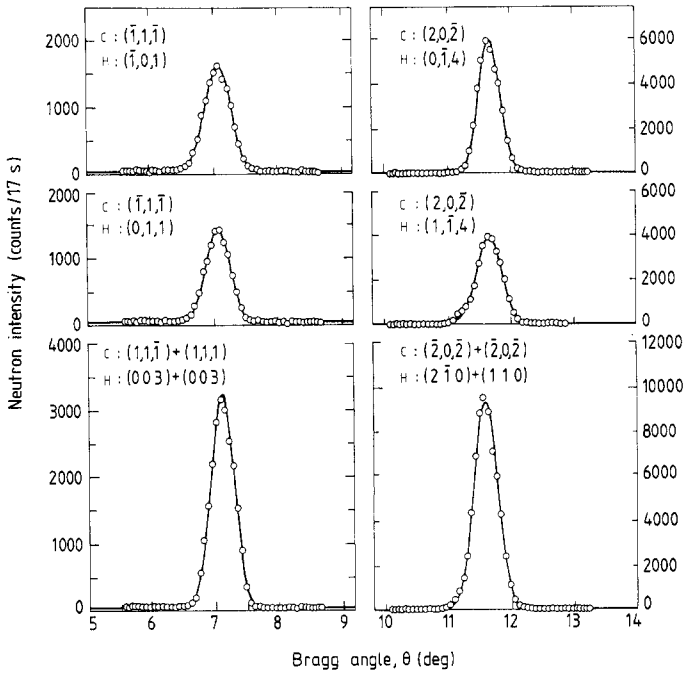

Figure 4. Examples of Bragg reflections in the UFe_2 crystal used in the neutron study. The Miller indices for both the FCC cubic cells (C) and the HCP pseudo-cell (H) are given. The top two curves show pure twin-A reflections, the middle two show pure twin-B reflections and the bottom two curves show reflections where both twins contribute to the scattering. The full curves are fits to gaussian line shapes. The pure twin-A or twin-B reflections are slightly wider than the combined reflections (see text).

Table 4. Examples of observed structure factors F^2_{obs} in the UFe_2. The observed intensities have been corrected for absorption using $\mu = 0.61\ cm^{-1}$. The Miller indices refer to a cubic lattice of the twin-A cell. The numbers in parentheses are the statistical uncertainties.

hkl	F^2_{obs}	*hkl*	F^2_{obs}	*hkl*	F^2_{obs}
111	485(5)	$\bar{2}22$	10525(35)	$\bar{3}33$	11650(40)
$\bar{1}11$	500(5)	$\bar{2}\bar{2}2$	11050(30)	$\bar{3}\bar{3}3$	12000(30)
$1\bar{1}1$	500(5)	$2\bar{2}\bar{2}$	10290(35)	$3\bar{3}\bar{3}$	11480(40)
$11\bar{1}$	900(5)	$22\bar{2}$	17915(35)	$33\bar{3}$	11870(30)
220	2790(15)	440	18860(60)	660	2365(25)
022	4120(15)	044	31360(60)	066	2135(20)
202	4230(15)	404	31785(55)	606	2040(20)
$2\bar{2}0$	4395(15)	$4\bar{4}0$	33740(60)	$6\bar{6}0$	2135(20)
$02\bar{2}$	2480(15)	$04\bar{4}$	19280(60)	$06\bar{6}$	2415(25)
$\bar{2}02$	2530(10)	$\bar{4}04$	19180(40)	$\bar{6}06$	2380(20)
400	3910(20)	800	16390(66)		
040	3715(15)	080	16040(60)		
004	3695(20)	008	15630(70)		

expected for the cubic symmetry. This could indicate either twinning or a change of symmetry from cubic to hexagonal.

2.2.1. Change of symmetry. Although the x-ray study seemed to support the assumption of cubic symmetry, let us consider for a moment the change to hexagonal symmetry. Transforming the FCC cubic cell with lattice constant a_c to a hexagonal cell results in a hexagonal cell with $a_h = b_h = \sqrt{2}/2a_c$ and $c_h = \sqrt{3}a_c$, with the hexagonal axis (c_h) parallel to the preferred $\langle 1,1,1\rangle$ axis, and the basal-plane hexagonal axes a_h and b_h parallel to the $\langle 1,\bar{1},0\rangle$ and $\langle 1,0,\bar{1}\rangle$ cubic axes perpendicular to the preferred cubic axis. Using a hexagonal cell given by $a = b = 4.989$ Å and $c = 12.220$ Å, an orientation matrix (UBMA)† could be calculated and the nine pairs of (2,2,0)-type cubic reflections could indeed be indexed in the hexagonal cell, either as $\langle 1,1,0\rangle$-type or as $\langle 1,0,4\rangle$-type hexagonal reflections. A set of about 1500 intensities was then collected at room temperature using the hexagonal orientation matrix. The incident neutron wavelength was 1.02 Å. The intensities were measured as $\omega - 2\theta$ scans with the χ-circle bisecting the scattering angle 2θ.

Table 5. Structure factors F^2_{obs} observed in the UFe_2 crystal with the spectrometer set at $(2\theta, \omega)$ for the (2,2,0)-type cubic reflection (see text). Using a hexagonal unit cell these reflections could be indexed as either (1,0,4)-type or (1,1,0)-type reflections (columns 1 or 4). Using a cubic unit cell they could all be indexed as (2,2,0)-type reflections (columns 3 or 6), but in this case the weaker intensities originate either from scattering by twin-A only or twin-B only, whereas scattering from both twin A and twin B contributes to the intensities in the strongest reflections. The numbers in parentheses are the statistical uncertainties. The cubic indices for the mixed reflections (marked (A + B)) refer to the twin-A cubic cell.

hkl (hexagonal)	F^2_{obs}	*hkl* (cubic)	*hkl* (hexagonal)	F^2_{obs}	*hkl* (cubic)
104	2480(15)	$02\bar{2}$(A)	110	4395(15)	$\bar{2}20$(A + B)
014	1830(15)	$02\bar{2}$(B)	$\bar{2}10$	4230(15)	202(A + B)
$\bar{1}14$	2790(15)	220(A)	$1\bar{2}0$	4120(15)	$\bar{2}\bar{2}0$(A + B)
$\bar{1}04$	2085(10)	220(B)			
$0\bar{1}4$	2530(10)	$20\bar{2}$(A)			
$1\bar{1}4$	1945(15)	$20\bar{2}$(B)			

Several symmetry-related reflections were measured, and although the intensities of reflections related by the hexagonal symmetry (see table 5) agree better than when comparing the intensities of reflections related by the cubic symmetry, it is obvious that the intensity difference between, for instance, (1,0,4) and (0,1,4) (hexagonal indexing) is considerably larger than that expected from statistical errors alone. Hence, it follows that the symmetry of the UFe_2 crystal cannot be hexagonal in complete agreement with the x-ray study.

2.2.2. Twinned crystal without change of symmetry. After having ruled out that there is a change of symmetry in UFe_2 from FCC cubic to a HCP structure, let us consider the possibility of a twinned cubic crystal. Using a cubic cell with $a = 7.055$ Å it was possible to find a cubic orientation matrix (UBMA) which could account for six of the (2,2,0)-

† For a description of the UB orientation matrix see Busing and Levy (1967).

type reflections found in the previously described systematic search. Another cubic UB matrix (UBMB) could account for the three remaining (2,2,0)-type reflections as well as three of the 2,2,0)-type reflections, which could also be accounted for by UBMA. Therefore, it is obvious that for the crystal symmetry to be cubic the UFe_2 crystal must be twinned. In table 5 we list the observed structure factors in UFe_2 for the nine (2,2,0)-type cubic reflections quoting both the hexagonal pseudo-cell indices and the cubic cell indices. The letters in parentheses indicate if either twin A or twin B or both twins contribute to the intensity of a particular reflection. In figure 4 we show as examples a few of the reflections in UFe_2. The reflections to which both twins contribute have approximately twice the intensity of the one-twin-only reflections, and are somewhat narrower. The fact that the one-twin-only reflections are broader than the combined reflections is presumably a consequence of the disorder in the crystal planes contributing to the one-twin-only reflections. This disorder is caused by the stacking faults introduced by the twinning, a disorder which does not exist in the crystal planes contributing to the combined reflections. The line broadening is similar to the line broadening observed in the so-called OD structures (order–disorder structures) of the Dornberger-Schiff-type (see, e.g., Jagner *et al* 1976 and references therein).

2.3. Structure refinement of twinned UFe_2

Having now established that the UFe_2 crystal is cubic and twinned, a structure refinement using the four-circle data could be performed. For this we used a modifed version of a standard crystallography program package (LINEX) supplied by the Department of Inorganic Chemistry, University of Aarhus, Denmark. The modifications were minor and only introduced to allow refinement of a twinned cubic structure.

At first, the 1500 reflections which had been collected at room temperature using the hexagonal UB matrix were converted to a set of 1500 reflections with cubic Miller indices. During this process each reflection was assigned a number (N) which indicates if the reflection is a twin-A-only reflection ($N_A = 1$), a twin-B-only reflection ($N_B = 4$) or a combined reflection ($N_{AB} = 2$). In the same process the intensities were corrected for absorption using a linear absorption coefficient of 0.61 cm^{-1}. Assuming a cubic Laves phase structure, a full-matrix least-squares refinement including isotropic extinction and anisotropic temperature factors was performed. In the refinement we allowed the scattering amplitude of the U atoms (b_U), the extinction parameter (R) and the temperature parameters (B^{ij}_U, B^{ij}_{Fe}) to vary. In addition the three scale factors SF_A, SF_B and SF_{A+B} were allowed to vary with the constraint $SF_{A+B} = \alpha(SF_A + SF_B)$. The scale factors are multipliers to the calculated intensities, in order to make the calculated intensities directly comparable to the measured intensities. This means that SF_A and SF_B are proportional to the volumes of twin A and twin B, respectively, and ideally $\alpha = 1$. However, a better fit was obtained if α was allowed to vary during the refinement giving $\alpha = 1.18$ for the best fit. In other words, the observed intensity of the one-twin-only reflections is too small when compared with the observed intensity of the mixed reflection. In order to explain this, we should again consider the disorder of the atoms in the crystal planes contributing to the one-twin-only reflections. As mentioned previously the disorder gives rise to line broadening which is included in the integrated peak intensity. However, the disorder will also give rise to diffuse intensity streaks which will result in increased background in some directions of reciprocal space. This diffuse intensity is not included in the measured peak intensity used in the refinement, and hence the one-twin-only reflections will be comparatively weaker than the mixed reflec-

Table 6. Results of structure refinement of 1500 reflections from twinned UFe_2 at room temperature using $b_{Fe} = 0.954 \times 10^{-12}$ cm. For a stoichiometric sample of UFe_2, $b_U = 0.8417 \times 10^{-12}$ cm. The extinction is less than 20% for the most extinct reflections, and typically between 5–10%. The index on the scale factors refers to the type of reflection.

Scattering amplitude	
b_U	$(0.843 \pm 0.003)\ 10^{-12}$ cm
Temperature factors (300 K)	
B_U	(0.91 ± 0.01) Å^2
B_{Fe}	(0.71 ± 0.01) Å^2
Scale factors	
SF_A	(7.8 ± 0.03)
SF_B	(6.9 ± 0.02)
α	(1.18 ± 0.01)
R factors	
$R(F)$	2.7%
$R(wF)$	2.5%
$R(F^2)$	3.5%
$R(wF^2)$	5.5%

tions. This phenomenon is also commonly observed in the OD Dornberger-Schiff (1966)-type structures.

After a few cycles, the refinement converged with an R factor for $|F|$ of $R(F) = 2.7\%$ ($R(wF) = 2.5\%$). The resulting parameters are listed in table 6. We find $b_U = (0.843 \pm 0.003) \times 10^{-12}$ cm. Using the accepted value for b_U of 0.8417×10^{-12} cm (Boeuf *et al* 1982), we find that the stoichiometry is (1.0015 ± 0.0035), i.e. the UFe_2 crystal is stoichiometric. The effect on the structural parameters of introducing the factor α were investigated in some detail by performing separate refinements of the data for twin-A-only, twin-B-only and mixed reflections. These refinements led to structural parameters similar to those quoted in table 6 with slightly better R factors ($R(F) \simeq 1.5\%$).

3. Polarised neutron experiments

3.1. Experimental details for the polarised neutron study

The polarised neutron experiments on the single crystal of UFe_2 were performed at the Orphée reactor, Laboratorie Léon Brillouin, Saclay, France. For this experiment we used the same crystal as that used in the unpolarised neutron study. The crystal was mounted in a superconducting vertical field cryo-magnet. A magnetic field of 2 T was applied along the vertical axis of the cylindrical crystal. The temperature was 10 K and the neutron wavelength 0.865 Å. The experiment consists of measuring the flipping ration R between Bragg intensities first with neutrons polarised (P) along the field $\boldsymbol{H}$ and then along $-\boldsymbol{H}$. A total of 110 flipping ratios were measured in the range $0.12\ \text{Å}^{-1} \leqslant \sin\theta/\lambda \leqslant 0.67\ \text{Å}^{-1}$. The R values were corrected for incomplete polarisation ($P_i = 0.980$) and for extinction based on the parameter extracted in § 2.3. The final averaged γ values, where $\gamma = M/N$ is the ratio of the magnetic to the nuclear structure factors, are given in table 7.

Table 7. Summary of polarised neutron data for UFe_2 at 10 K and 2 T. N is the nuclear structure factor per formula unit of UFe_2, γ is determined experimentally, M is determined from equation (3) using $b_U = 0.8417 \times 10^{-12}$ cm and $b_{Fe} = 0.954 \times 10^{-12}$ cm and have been corrected for isotropic temperature factors and extinction. The product $\mu f(Q)$ for iron is derived assuming $\mu_{Fe} f(Q) = \mu_{Fe}\langle j_0(Q)\rangle$, with $\mu = 0.60(1)\ \mu_B$ and $\langle j_0\rangle$ is taken for the Fe^{2+} configuration. The uranium amplitude $\mu f(Q)$ is shown in figure 6. The nuclear structure factor N attains the values in order of increasing strength $a = b_{Fe} - b_U/\sqrt{2}$, $b = b_U$, $c = 2b_{Fe} - b_U$, $d = b_{Fe} + b_U/\sqrt{2}$, $e = 2b_{Fe}$ and $f = 2b_{Fe} + b_U$.

hkl	Sin θ/λ ($Å^{-1}$)	N	γ	M (μ_B)	$(\mu f)_{Fe}$ (μ_B)	$(\mu f)_U$ (μ_B)
111	0.123	a	0.378(7)	0.50 (1)	0.516	0.018(7)
220	0.200	$-b$	0.0128(5)	−0.040(2)		0.040(2)
311	0.235	$-d$	0.071(2)	−0.41 (1)	0.367	0.06 (1)
222	0.245	e	0.103(2)	0.73 (2)	0.353	
400	0.283	c	0.137(4)	0.54 (2)	0.299	0.05 (1)
331	0.309	$-a$	0.164(4)	−0.218(5)	0.265	0.067(8)
422	0.347	b	0.016(1)	0.051(3)		0.051(3)
511	0.368	d	0.041(2)	0.23 (1)	0.196	0.05 (1)
333	0.368	d	0.038(2)	0.22 (1)	0.196	0.03 (1)
440	0.401	f	0.038(1)	0.39 (1)	0.166	0.06 (1)
531	0.419	$-a$	0.090(7)	−0.12 (1)	0.148	0.046(9)
620	0.448	b	0.015(3)	0.048(8)		0.048(8)
533	0.465	$-d$	0.023(1)	−0.135(6)	0.115	0.028(8)
622	0.470	e	0.034(2)	0.24 (1)	0.112	
551	0.506	a	0.053(3)	0.070(4)	0.090	0.028(5)
642	0.530	$-b$	0.009(2)	−0.028(6)		0.028(6)
553	0.544	$-d$	0.015(2)	−0.09 (1)	0.070	0.03 (1)
731	0.544	$-d$	0.017(2)	−0.010 (1)	0.070	0.04 (1)
660	0.601	$-b$	0.010(2)	−0.031(6)		0.031(6)
751	0.614	$-d$	0.009(2)	−0.05 (1)	0.042	0.01 (1)
662	0.618	e	0.010(2)	0.07 (1)	0.041	

3.2. Examination of the magnetic anisotropy

The correct expression for the flipping ratio is

$$R = [N^2 + 2(\boldsymbol{P}\cdot\boldsymbol{q})NM + (\boldsymbol{q}\cdot\boldsymbol{q})M^2]/[N^2 - 2(\boldsymbol{P}\cdot\boldsymbol{q})NM + (\boldsymbol{q}\cdot\boldsymbol{q})M^2] \tag{3}$$

where $\boldsymbol{P}$ is the neutron polarisation vector and

$$\boldsymbol{q} = \boldsymbol{Q} \times (\mu \times \boldsymbol{Q}) \tag{4}$$

is the magnetic interaction involving the unit scattering vector $\boldsymbol{Q}$ and the precise direction of the magnetic moment through the unit vector $\hat{\mu}$ along the moment direction. Equation (4) selects the component of the magnetisation perpendicular to the scattering vector $\boldsymbol{Q}$. Recall that $|\boldsymbol{Q}| = 4\pi \sin\theta/\lambda$, where θ is the Bragg angle and λ the neutron wavelength. For a more complete description of the consequences of equation (3) see Wulff *et al* (1988), where we have exploited the geometrical properties of equation (3) to prove the extremely high anisotropy of $PuFe_2$. In this latter compound the moments are locked along the $\langle 1,0,0\rangle$ axis closest to the applied magnetic field.

In UFe_2 we are working with a twinned crystal so the situation is more complex than in $PuFe_2$ (Wulff *et al* 1988). Let us first examine a set of Bragg reflections from twin A alone. The question is whether the magnetic moments are parallel to the field direction

or to the closest ⟨1,1,1⟩ axis, which in this case is only 7.5° away from the field. Because the values of γ should depend only on the Miller indices, the method of doing this is to examine the consistency of the γ values for a particular set of nominally equivalent (h,k,l) values, but with different assumptions as to the direction of $\hat{\mu}$ in equation (1). The $\gamma(H)$ values, i.e. those values derived by assuming $\mu \| \boldsymbol{H}$ for the individual reflections from twin A (marked A), twin B (marked B, non-integer cubic Miller indices) or from mixed reflections (marked A + B) in the ⟨2,2,0⟩ and ⟨3,1,1⟩ sets are given in table 8. It can immediately be seen that the γ values are extremely consistent. As shown in Wulff *et al* (1989b) the χ^2 values for the ⟨3,1,1⟩ twin-A reflections is 2.8 for $\mu \| \boldsymbol{H}$, whereas $\chi^2 = 17$ for $\mu \| [1,\bar{1},1]$. This shows that $\mu \| \boldsymbol{H}$ for twin A. The same analysis may be performed for twin B or for the mixed reflections, showing beyond all doubt that $\mu \| H$ in the whole crystal. This is in spite of the 31° between $\boldsymbol{H}$ and the nearest ⟨1,1,1⟩ axis in twin B.

By examining reflections from the U and Fe sublattices separately we may determine if they behave differently (see Wulff *et al* 1988); but we find, as expected, that both the uranium and iron moments in UFe_2 are directed along the applied field direction. UFe_2 is thus magnetically soft in agreement with Popov *et al* (1980). These authors show that although UFe_2 exhibits a rhombohedral distortion of approximately 40% of that found in $NpFe_2$ (Knott *et al* 1980), the magnetic anisotropy is extremely small. The easy axis is indeed ⟨1,1,1⟩, but the magnetic anisotropy constant $K_1 = -10^6$ erg cm^{-3} at 10 K. This value is comparable to that found in pure Fe and approximately three orders of magnitude less than the low-temperature values found for $TbFe_2$ (-5×10^8 erg cm^{-3}) or estimated for $NpFe_2$ (-10×10^9 erg cm^{-3}). It might be mentioned that although the rhombohedral distortion is large it is too small to be observed at the neutron diffractometers used for the present measurements.

Table 8. Individual values of R (flipping ratio), q^2 (interaction vector, see equation (4)) and $\gamma(H)$ where $\mu \| \boldsymbol{H}$ in equation 4. The average values for twin A, twin B and the mixed reflections are given in the last column. The structure factor per formula unit is b_U for the ⟨2,2,0⟩ and $b_U/\sqrt{2} + b_{Fe}$ for the ⟨3,1,1⟩.

hkl	Twin	R_{obs}	q^2	γ	Mean-value γ
$\bar{2}\bar{2}0$	A	1.046(3)	0.9866	0.013(1)	
220	A	1.045(5)	0.9866	0.012(1)	0.013(1)
$20\bar{2}$	A	1.044(4)	0.9883	0.013(1)	
$2/3\ \bar{2}/3\ 2/3$	B	1.031(6)	0.8445	0.010(2)	0.010(2)
022	A + B	1.053(3)	0.999	0.014(1)	0.013(1)
$0\bar{2}\bar{2}$	A + B	1.045(4)	0.9999	0.012(1)	
$\bar{1}\bar{3}1$	A	1.205(4)	0.8246	0.068(1)	
$1\bar{1}3$	A	1.216(2)	0.8190	0.071(1)	0.070(2)
113	A	1.182(5)	0.7251	0.069(1)	
$31\bar{1}$	A	1.243(3)	0.9100	0.072(1)	
$5/3\ 5/3\ 7/3$	B	1.202(4)	0.7959	0.069(1)	0.069(1)
$\bar{7}/3\ 1/3\ 7/3$	B	1.261(7)	0.9969	0.069(1)	
$\bar{1}13$	A + B	1.273(2)	0.9867	0.073(1)	
131	A + B	1.271(3)	0.9896	0.072(1)	
311	A + B	1.156(4)	0.6198	0.070(1)	0.072(1)
$3\bar{1}\bar{1}$	A + B	1.159(3)	0.6280	0.071(1)	
$\bar{1}3\bar{1}$	A + B	1.269(2)	0.9896	0.072(1)	

We are readily able to verify that K_1 is indeed small by examining the terms giving the magnetic anisotropy. The energy is given by

$$E = K_1(\alpha_1^2\alpha_2^2 + \alpha_2^2\alpha_3^2 + \alpha_3^2\alpha_1^2) - \mu H \cos\theta \tag{5}$$

where α_i are direction cosines between the moment direction and the three cube axes. In equation (5) K_1 is the leading anisotropy term:

$$K_1 = K_1^0 + \Delta K_1^{me} \tag{6}$$

where K_1^0 is the intrinsic anisotropy and ΔK_1^{me} is the magneto-elastic contribution. The applied field is $\boldsymbol{H}$ and θ is the angle between $\boldsymbol{H}$ and the magnetic moment μ. If we neglect higher-order terms and use units of K mol^{-1} (note that 1 $\mu_B = 0.93 \times 10^{-20}$ EMU) equation (4) gives

$$E = -0.313\Sigma - 1.44 \cos\theta \text{ K mol}^{-1}$$

where Σ is the product of direction cosines defined in equation (5). As is well known, $\Sigma = 1/3$ for $\mu \| \langle 1,1,1 \rangle$ and has its minimum value of zero for $\mu \| \langle 1,0,0 \rangle$. We have used $\mu = 1.09\ \mu_B$ mol^{-1} as measured by Aldred (1979) and an applied field of 2 T.

As can be readily seen from equation (5) the second term dominates and the minimum energy is thus when $\theta = 0$, $\mu \| \boldsymbol{H}$. Thus in both twin A, where the angle between the field and the nearest $\langle 1,1,1 \rangle$ is $\sim 8°$, and in twin B, where the angle is 31.5°, the moment rotates to be parallel to $\boldsymbol{H}$. Unfortunately, our data do not allow us to give a reliable upper limit of K_1, but an estimate is $|K_1| \leqslant 5 \times 10^6$ erg cm^{-3}. Clearly, this method of investigation may be applied to other systems where for large $|K_1|$ values the moment might be expected to lie midway between $\boldsymbol{H}$ and the easy axis.

Popov *et al* (1980) have gone further and shown that ΔK_1^{me} must be large because of the large spontaneous rhombohedral distortion in UFe_2. They quote $\Delta K_1^{me} \simeq -8 \times 10^6$ erg cm^{-3} at 5 K. From equation (4), $K_1^0 \simeq +7 \times 10^6$ erg cm^{-3}. As discussed by Clark (1980) the ratio $\Delta J_1^{me}/J_1^0$ is normally less than 0.25, but it is greater than 1 in UFe_2. This is what is unusual in UFe_2 and further investigation of this point by other microscopic techniques would seem worthwhile. It may also be a point worth considering from the viewpoint of the band-structure calculations. Certainly, through its coupling to the lattice, the small orbital moment of 0.23 μB is primarily responsible in driving the rhombohedral distortion.

3.3. Determination of the magnetic moments and the form factors

The magnetic structure factors listed in table 7 may be separated into contributions from the Fe and U sublattices. We plot the magnetic scattering amplitude for the Fe sublattice as a function of Q in figure 5. The full curve is the experimental form factor for elemental Fe (Shull and Yamada 1962, Shull and Mook 1966) which, when fit to the points, extrapolates to 0.60(1) μ_B per Fe atom. We note that the iron atom in the Laves phase is not at a site of cubic symmetry (Givord *et al* 1980) so that a factor $\langle j_2 \rangle$ must be included in the analysis. This arises from any small orbital moment on the Fe atom. We have included this in our analysis and find that the orbital moment at the Fe site is +0.01(2) μ_B. This is lower than the value of +0.07 μ_B calculated by Brooks *et al.* (1988). In our further analysis we neglect any orbital contribution at the Fe site. Note that the open circles have a contribution from the Fe atoms only, and therefore are not subject to any uncertainty as to the contribution from the U sublattice. This value of 0.60(1) μ_B is in

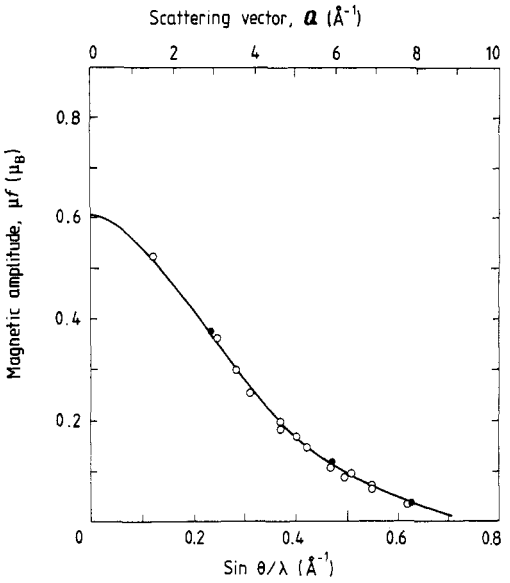

Figure 5. Magnetic scattering amplitude from the Fe sublattice as a function of sin θ/λ. The full symbols have no contribution from the U sublattice. The full curve is that for Fe metal normalised to 0.60 μ_B.

excellent agreement with that of 0.59(2) μ_B determined on polycrystalline material of a stoichiometric sample. Table 9 summarises the magnetic moments found in UFe_2.

The magnetic scattering amplitude for the U sublattice is shown in figure 6. As noted before, the form factor is highly unusual with an extrapolation at $Q = 0$ to $\mu \simeq 0\ \mu_B$, and more details of the physics that this implies may be found in Wulff *et al* (1989a, b). For

Table 9. Values for the different magnetic moments as discussed in the text. μ_U and μ_{Fe} are the total moments on uranium and iron, respectively, μ_{spd} is the conduction-electron moment deduced using the total neutron moment and the magnetisation value of 0.965(3) μ_B as deduced in the magnetisation experiment. μ_l and μ_s are the individual orbital and spin contributions to the U moment.

	Previous work			
(μ_B)	a	b	Present work	Theory c
μ_U	0.03(1)	0.06(1)	0.01(1)	−0.11
μ_{Fe}	0.38(2)	0.59(2)	0.60(1)	0.80
μ_{spd}	—		−0.25(2)	−0.09
U atom				
μ_l	—	—	0.23(2)	0.47
μ_s	—	—	−0.22(2)	−0.58

[a] Yessik (1969).
[b] Lander *et al* (1977).
[c] Brooks *et al* (1988).

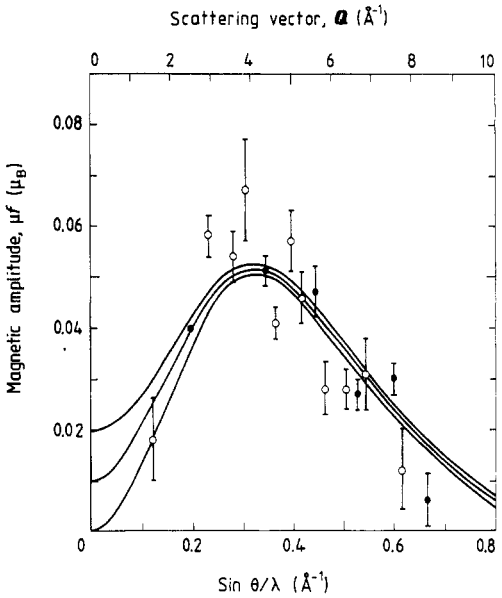

Figure 6. The magnitude of the magnetic scattering on the U sublattice as a function of sin θ/λ ($=Q/4\pi$). The extrapolation to $Q = 0$ gives the magnetic moment. The full symbols are from Bragg reflections coming from the U sublattice only. The open symbols come from Bragg reflections that have both U and Fe contributions, but the Fe contribution has been subtracted. The full central curve is the fit to equation (7) with the outer curves representing the limits defined by the error bars and the strong correlation between μ and C_2.

completeness we illustrate the analysis briefly here. In the dipole approximation

$$\mu f(Q) \simeq \mu_s\langle j_0\rangle + \mu_l(\langle j_0\rangle + \langle j_2\rangle) \tag{7}$$

where μ is the total moment, μ_s is the spin component, normally $2\langle S\rangle$, μ_l is the orbital component, normally $\langle L\rangle$, and $\langle j_0\rangle$, $\langle j_0\rangle$ and $\langle j_2\rangle$ are Bessel transforms of the single 5f electron charge-density distribution $U^2_{5f}(r)$. Since $\mu = \mu_s + \mu_l$ we rearrange equation (7) to give

$$\mu f(Q) = \mu(\langle j_0\rangle + C_2\langle j_2\rangle) \tag{8}$$

where $C_2 = \mu_l/\mu$. The functions $\langle j_0\rangle$ and $\langle j_2\rangle$ are tabulated by Desclaux and Freeman (1978) so that we may readily least-squares refine the experimental values of $\mu f(Q)$, the magnetic scattering amplitude, against μ and C_2. Unfortunately, the shape of this curve leads to strong correlations between μ and C_2, and we illustrate the best fit and two extremes in figure 6. We find $\mu = 0.01(1)\ \mu_B$ and $C_2 = 23(1)$, leading to $\mu_l = 0.23(1)\ \mu_B$ and $\mu_s = -0.22(2)\ \mu_B$ in equation (7).

It is important to emphasise that the full symbols in figure 6 come from the U sublattice only, and using them alone gives the *same* values for μ_l and μ_s. For the other points the Fe contribution must be subtracted. Since the Fe contribution is much larger (by a factor of at least ten at most Q values) the assignment of error bars in figure 6 has to be treated with caution. As an example we have tried analysing for an asymmetric form factor on the Fe site as suggested by Yessik (1969), but find that it is not statistically significant. The same situation was found for $PuFe_2$ by Wulff *et al* (1988). However, it is known from work by Aldred (1979) on Yessik's UFe_2 crystals that they were non-

stoichiometric so his UFe_2 form factors do not necessarily agree with our form factors for stoichiometric UFe_2. Nevertheless, the distribution of points in figure 6 does appear to indicate asphericity in the uranium $f(Q)$. Despite this, we do not presently find further analysis of our UFe_2 data warranted. The reason for this is two-fold. Firstly, one should go further than the dipole approximation in equation (7), especially for $\sin\theta/\lambda > 0.4$ Å^{-1}. Secondly, and perhaps more important, we believe it is necessary to re-examine the fundamental cross section that gives rise to equation (3). Equation (3) is based on the assumption that the total moment μ is a scalar quantity independent of $\boldsymbol{Q}$, i.e. that the sum $\mu = \mu_l + \mu_s$ is independent of $\boldsymbol{Q}$. In localised lanthanide systems this is a correct assumption. However, Brooks *et al* (1988) have shown that the 5f electrons are itinerant and that, whereas μ_l is a well defined quantity when integrated over the Brillouin zone, it may well vary in direction and magnitude for a particular Fourier component. This is clearly not a large effect, otherwise no smooth curve could fit the data of figure 6, but without further theoretical consideration of this point it is unreasonable to proceed with a more sophisticated analysis of the U form factor.

4. Field and temperature dependence of magnetic moments

We show in figure 7 the magnetic moment as a function of magnetic field as measured on an identical crystal (and orientation) to that used in the neutron study. These measurements were performed at the Service National des Champs Intenses, Grenoble.

The moment induced by 2 T is 0.965(3) μ_B, which has to be compared with the neutron value of $2\mu_{Fe} + \mu_U = 1.20(2) + 0.01(2) = 1.21(3)\ \mu_B$. We note that the value of 0.965 μ_B is lower than the value of 1.05 μ_B found by Aldred (1979) and that of 1.158 μ_B found by Andreev *et al* (1979). We have no simple explanation for this discrepancy. Aldred (1979), who did a careful study of different crystals with different stoichiometries, also notes that all samples contain small amounts of free iron. We feel the discrepancies are rather large to be explained by such impurities, which would not affect the neutron results, but we cannot exclude them. As shown by Aldred (1979), the moment drops when one moves off stoichiometry but both our neutron refinement, the lattice par-

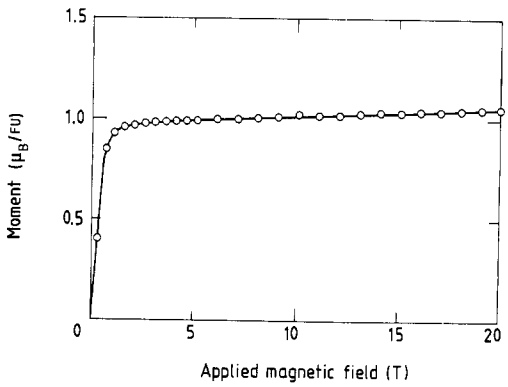

Figure 7. Magnetisation against applied magnetic field at 10 K for the same crystal as used in the neutron study. The magnetic field was applied along the same axis as in the polarised neutron study, i.e. approximately 7.5° away from the [1$\bar{1}$1] axis of twin A (see text).

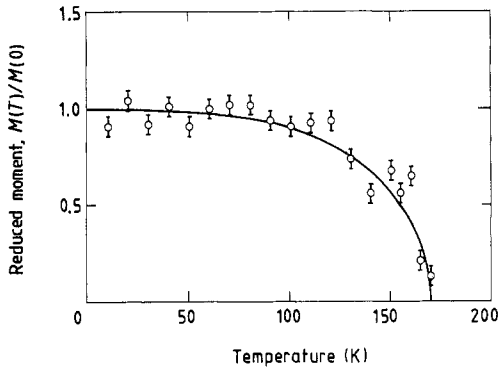

Figure 8. Temperature dependence of the reduced magnetic moment in UFe_2 measured by unpolarised neutron diffraction. The data have been deduced from the integrated intensity of the (1,1,1) reflection. The nuclear scattering has been subtracted using a high-precision measurement of the flipping ratio at 10 K. The full curve is the normalised $S = 1/2$ Brillouin function.

ameter (x-ray data) and T_c (see below) show that our sample is very close to stoichiometry. It is interesting to note that our high-field susceptibility, as deduced from figure 7, is $6.4(5) \times 10^{-6}$ EMU g^{-1}. This is in good agreement with the values between 5×10^{-6} EMU g^{-1} and 9×10^{-6} EMU g^{-1} given by Aldred, deduced with much lower magnetic fields. Such a high value of χ in the ordered state is consistent with itinerant magnetism.

In figure 8 we show the temperature dependence of the magnetic contribution to the (1;1,1) reflection. The data have been deduced from a set of unpolarised integrated intensities of the (1,1,1) reflection after subtracting the nuclear scattering contribution determined from a high-precision measurement of the flipping ratio of the (1,1,1) peak at 10 K. In reality the (1,1,1) measures a combination $(\mu_{Fe} - 1\sqrt{2}\mu_U)$ of the moment on the U and the Fe sublattices. However, measurements at 2 T of the temperature dependence of the flipping ratios of the (2,2,0) peak, which measures the uranium moment only, and of the (2,2,2) peak which measures the iron moment only, show that within statistics the two moments have the same temperature dependencies. Therefore, it is justified to claim that figure 8 represents the temperature dependence of the total ordered moment in UFe_2. The Curie temperature is seen to be 170(5) K, which is essentially the same as the value deduced by Aldred (1979) for stoichiometric UFe_2.

The theories of Brooks *et al* (1988) predict a different pressure effect for μ_l and μ_s, because the hybridisation is a function of interatomic spacing. However, the variation of the intra-atomic exchange interaction, which is responsible for the spontaneous ordering, is too small an energy to give measurable effects in μ_l and μ_s, so we would indeed expect the ordered moments on the two sublattices to behave similarly with temperature, as found by the flipping ratio measurements.

5. Conclusion

This study was performed on a twinned crystal of UFe_2 with two twins of roughly the same volume. Although not normally recommended for diffraction studies, we have been able to utilise the twinning to further investigate the magnetic anisotropy.

The crystal is shaped as a cylinder and cut from a large boule with a $\langle 1,1,1\rangle$ axis (determined by x-rays) nearly parallel to the cylinder axis. However, this axis is not the twin axis. In fact, the twin axis lies nearly in the radial plane of the cylinder, about 70° from the cylinder axis, and the cylinder axis is 7.5° away from the $[\bar{1},1,\bar{1}]$ axis in twin A which is perfectly aligned with the $[\bar{1},\bar{1},\bar{5}]$ axis of twin B. For twin B, the $[\bar{1},\bar{1},\bar{3}]$ direction is only ~2° away from the vertical field direction. In the polarised neutron study, the field was aligned along the cylinder axis, and the field was not applied along the same crystallographic direction in the two twins. In twin A, the field was nearly parallel to the $[\bar{1},1,\bar{1}]$ direction and in twin B slightly better aligned along the $[\bar{1},\bar{1},\bar{3}]$ direction. If UFe_2 is magnetically anisotropic, the anisotropy will manifest itself in a polarised neutron study by different magnetic structure factors for equivalent reflections from twin A or twin B (or for combined reflections). We measured the flipping ratios of several types of equivalent reflections from twin A, twin B or both twins. In each case they reduce to equivalent magnetic structure factors only if the moment direction is assumed to be parallel to the applied magnetic field. Essentially, with a twinned crystal we are performing two magnetisation experiments simultaneously. The early part of this paper discusses the geometry of the twinning, and we do this in some detail so that it may be of help to others faced with the same problem.

As shown in table 9 the conduction-electron polarisation (μ_{spd}) takes a reasonably large value of $-0.25(2)\ \mu_B$ per formula unit. It is significantly larger than that found in ferromagnets such as US (Wedgwood 1972) where the value is $-0.15\ \mu_B$. We ascribe this large value to hybridisation effects involving the transition-metal electrons, and it is interesting to note the value of $-0.31\ \mu_B$ in $LuFe_2$ (Givord *et al* 1980), and the large value suggested by experiments on $NpFe_2$ and $PuFe_2$ (Aldred *et al* 1975). Note that this is difficult to calculate theoretically so the disagreement between theory and experiment in table 9 is not surprising.

Given the large value of μ_{spd} we can also ask whether this could affect the analysis of the form factor on the U site. The answer is negative. First, we anticipate that most of the responses come from 4s electrons originating from the iron atoms, and this is well known to have a form factor that drops to zero by $\sin\theta/\lambda \simeq 0.1\ \text{Å}^{-1}$ (Shull and Yamada 1962). If we take, for example, $\sim -0.1\ \mu_B$ associated with the U 6d–7s electrons, then even the free-atom form factor (Freeman *et al* 1976) falls to zero by the $\boldsymbol{Q}$ value of the (2,2,0) reflection. Second, the form factor of these electrons will fall off even more steeply when solid-state effects are included, so that at the (1,1,1) reflection any possible contribution can be estimated as less than $0.006\ \mu_B$, i.e. comparable to the error bar. In summary, it is clear that conduction-electron effects cannot be responsible for the unusual form factor at the U site (figure 6).

The most important conclusion of the present work is the confirmation of the prediction of Brooks *et al* (1988) that the orbital and spin moments almost cancel on the uranium sublattice in UFe_2. This results in a most unusual form factor (figure 6). Earlier experiments on UFe_2 by Yessik (1969) and Lander *et al* (1977) were not aware of this form factor, indeed it is almost a unique situation, and hence their extrapolation to $\boldsymbol{Q} = 0$ to obtain the U moment are incorrect. Yessik's samples, according to work done on them by Aldred (1979), were non-stoichiometric and hence the Fe moment given in table 9 must also be suspect.

At first sight the comparison with theory in table 9 might seem poor, but the important point to realise is that theory predicts μ_U is smaller than either μ_l or μ_s. At this stage the theoretical calculations suggest the net moment is antiparallel to the Fe moment, and further refinements are clearly required to predict even smaller values of μ_l and μ_s. This,

however, should not obscure the excellent overall trends which represent a new effect in orbital magnetism.

Acknowledgments

The conscientious help of Mogens H Nielsen during the data collection is gratefully acknowledged. Special thanks are due to Rita Hazell for her help and advice in adopting the structure refinement programme to refine twinned structures. We thank C Rijkeboer for preparing the crystal used in this study, and we have benefitted from many stimulating discussions with M Brooks and J Schweizer. Finally we wish to thank Maurice Guillot at the Service National des Champs Intenses, Grenoble, for his assistance during the magnetisation measurements.

References

Aldred A T 1979 *J. Magn. Magn. Mater.* **10** 42
Aldred A T, Dunlap B D, Lam D J, Lander G H, Mueller M H and Nowik I 1975 *Phys. Rev.* B **11** 530
Andreev A V, Deryagin A V, Levitin R Z, Markosyan A S and Zeleny M 1979 *Phys. Status Solidi* a **52** K13
Boring A M, Albers R C, Schadler G H, Lawson A C, Weinberger P and Christensen N E 1987 *Phys. Rev.* B **36** 5507
Boeuf A, Caciuffo R, Renato R, Rustichelli F, Fournier J M, Kischko U and Manes L 1982 *Phys. Rev. Lett.* **49** 1086
Brooks M S S, Eriksson O, Johansson B, Franse J J M and Frings P H 1988 *J. Phys. F: Met. Phys.* **18** L33
Busing W R and Levy H A 1967 *Acta Crystallogr.* **22** 457; or 1974 *International Tables for X-ray Crystallography IV* (Birmingham, UK: Kynoch Press) p 276
Clark A E 1980 *Ferromagnetic Materials* ed. E P Wohlfarth (Amsterdam: North-Holland) p 531
Desclaux J P and Freeman A J 1978 *J. Magn. Magn. Mater.* **8** 119
Dornberger-Schiff K 1966 *Lehrgang über OD-Strukturen* (Berlin: Academie)
Eriksson O, Johansson B, Skriver H L and Brooks M S S 1986 *Physica* B **144** 32
Franse J J M 1983 *J. Magn. Magn. Mater.* **31–34** 819
Freeman A J, Desclaux J P, Lander G H and Faber J 1976 *Phys. Rev.* B **13** 1168
Giebultowicz T M, Rhyne J J, Ching W Y, Huber D L, Furdyna J K, Lebech B and Galazka R R 1989 *Phys. Rev.* B **39** 6857
Givord D, Gregory A R and Schweizer J 1980 *J. Magn. Magn. Mater.* **15–18** 293
Henriksen K, Larsen F K and Rasmussen E 1986 *J. Appl. Crystallogr.* **19** 390
Jagner S, Hazell R, Grønbæk H and Larsen H P 1976 *Acta Crystallogr.* B **32** 548
Knott H W, Lander G H, Mueller M H and Vogt O 1980 *Phys. Rev.* B **21** 4159
Lander G H, Aldred A T, Dunlap B D and Shenoy G K 1977 *Physica* B **86–88** 152
Popov Y F, Levitin R Z, Zeleny M, Deryagin A V and Andrev A V 1980 *Sov. Phys.-JETP* **51** 1223
Shull C G and Mook H A 1966 *Phys. Rev. Lett.* **16** 184
Shull C G and Yamada Y 1962 *J. Phys. Soc. Japan* **17** 1
Steigenberger U, Lebech B and Galazka R 1986 *J. Magn. Magn. Mater.* **54–57** 1285
Wedgwood F A 1972 *J. Phys. C: Solid State Phys.* **5** 2427
Wulff M, Lander G H, Lebech B and Delapalme A 1989a *Phys. Rev.* **337** 4719
Wulff M, Lander G H, Rebizant J, Spirlet J C, Lebech B, Broholm C and Brown P J 1988 *Phys. Rev.* B **37** 5577
Wulff M, Lebech B, Delapalme A, Lander G H, Rebizant J and Spirlet J C 1989b *Physica* B **156 + 157** 836
Yessik M 1969 *J. Appl. Phys.* **40** 1133